# Intra- and intermolecular interactions in substituted dithia[3.3]metacyclophanes

**Tetsuji Moriguchi,* Kazunori Sakata and Akihiko Tsuge***

*Department of Applied Chemistry, Faculty of Engineering, Kyushu Institute of Technology, 1-1 Sensui-cho, Tobata-ku, Kitakyushu 804-8550, Japan*

***Received (in Cambridge, UK) 2nd January 2001, Accepted 23rd March 2001***
***First published as an Advance Article on the web 18th April 2001***

The conformational properties of and intramolecular hydrogen-bonding in dithia[3.3]metacyclophanes carrying one or two amino groups on their internal positions were examined by their $^1$H-NMR and IR spectra and by X-ray structural analyses. It was suggested that an intramolecular hydrogen-bonding network between the amino protons and bridge sulfur atoms is closely related to the conformations of the cyclophanes. Crystal structural analyses of dithia[3.3]metacyclophanes carrying an amino and a nitro group on their internal positions were also carried out. It has been found that the molecules assemble as one-dimensional array columns in the crystal owing to the intermolecular π–π interaction and this columnar structure is deformed by the occurrence of intermolecular hydrogen-bonding.

## Introduction

Recently, weak interactions such as hydrogen-bonding, π–π interactions, and charge-transfer interactions have attracted much attention from organic, biological and physical chemists,[1] because they play very important roles in supramolecular aggregates. Small-sized metacyclophanes, which are characterized by a specific transannular interaction, could be unique candidates for the study of such weak inter- and intramolecular interactions.[2] Böckmann and Vögtle reported preparative methods for various kinds of dithia[3.3]metacyclophanes (MCPs) and related compounds.[3] These MCPs seem to be very suitable for the investigation of weak interactions since two aromatic rings and the substituents on the MCPs are located in close proximity. Böckmann and Vögtle studied the transannular interactions in these compounds by means of their electronic spectra,[4] however, a detailed study of the molecular and crystal structure of dithia[3.3]MCP in terms of the weak interactions has not yet been carried out.

In this paper, we report the preparation of dithia[3.3]MCPs having electron-releasing and -withdrawing substituents on their internal positions and discuss their structural properties in order to evaluate the weak interactions. Furthermore, their molecular and crystal structures were studied from the viewpoint of intra- and intermolecular π–π interactions or hydrogen-bonding properties.

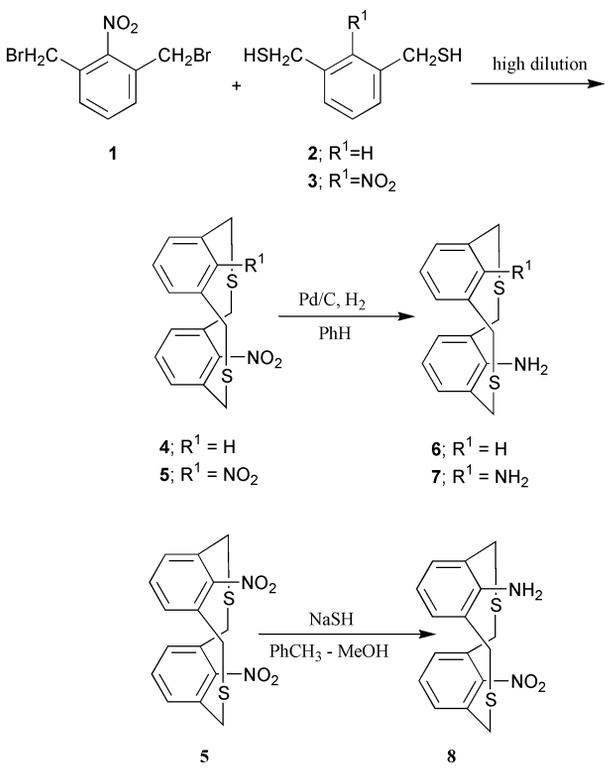


**Scheme 1**

## Results and discussion

2,6-Bis(bromomethyl)nitrobenzene **1**, 1,3-bis(mercaptomethyl)-benzene **2** and 2,6-bis(mercaptomethyl)nitrobenzene **3** were prepared according to the previously outlined procedure.[4] Nitrodithia[3.3]MCPs **4** and **5** were prepared from the corresponding bromomethyl **1** and mercaptomethyl compounds **2** and **3**, respectively by using the high-dilution technique.[5] Nitrodithia[3.3]MCPs **4** and **5** were readily reduced with hydrogen gas in the presence of 10% Pd/C as a catalyst to give monoamino **6** and diaminodithia[3.3]MCP **7** in quantitative yield, respectively. Aminonitrodithia[3.3]MCP **8** was prepared from dinitrodithia[3.3]MCP **5** by the partial reduction with sodium hydrosulfide in methanol–toluene mixed solvent in a yield of 45% (Scheme 1). These MCPs were characterized by their $^1$H-NMR and IR spectra and also by MS and elemental analyses. Some of their spectral data are summarized in Table 1.

In their $^1$H-NMR spectra, MCPs **5** and **7**, which have a symmetric structure, display a pair of doublets for their bridge protons. In MCPs **4**, **6** and **8**, which are asymmetric molecules, two pairs of doublets were observed. In detail, one of the coupling constants in **4** and **8** ($J$ = 15.3 Hz) is the same as the corresponding constants in **5** and **7**. The coupling pattern in **4** is also identical with that in **8**. In contrast, MCP **6** exhibits a different coupling pattern and coupling constants from those of **4** and **8**. Such differences probably come from the conformational character of the MCPs. The internal aryl proton of

 DOI: 10.1039/b100285f

**Table 1** Selected spectral data of dithia[3.3]MCPs **4**–**8**

| MCP | Chemical shift[a](ppm) Bridge-H | Internal Ar–H | $\nu(NH_2)$[b]/cm$^{-1}$ |
|---|---|---|---|
| **4** | 3.61 (d, $J$ = 14.7 Hz), 3.73 (d, $J$ = 15.3 Hz), 4.05 (d, $J$ = 15.3 Hz), 4.20 (d, $J$ = 14.7 Hz) | 7.36 | |
| **5** | 3.58 (d, $J$ = 15.3Hz), 4.52 (d, $J$ = 15.3 Hz) | | |
| **6** | 3.39 (d, $J$ = 14.3 Hz), 3.68 (d, $J$ = 14.3 Hz), 3.82 (d, $J$ = 13.7 Hz), 4.05 (d, $J$ = 13.7 Hz) | 4.93 | 3390, 3322 |
| **7** | 3.88 (d, $J$ = 15.3 Hz), 4.14 (d, $J$ = 15.3 Hz) | | 3395, 3375, 3320 |
| **8** | 3.74 (d, $J$ = 14.7 Hz), 3.83 (d, $J$ = 15.3 Hz), 4.02 (d, $J$ = 15.3 Hz), 4.46 (d, $J$ = 14.7 Hz) | | 3450, 3361 |

[a] In $CDCl_3$. [b] In KBr.

**Table 2** Selected bond lengths (Å) and bond angles (°) for MCP **6**

| | |
|---|---|
| S(1)–C(1) | 1.836(5) |
| S(1)–C(2) | 1.855(6) |
| S(2)–C(9) | 1.836(6) |
| S(2)–C(10) | 1.852(5) |
| N(1)–C(8) | 1.421(6) |
| | |
| C(1)–S(1)–C(2) | 104.3(2) |
| C(9)–S(2)–C(10) | 104.4(2) |
| C(8)–N(1)–H(16) | 119(3) |
| C(8)–N(1)–H(17) | 111(5) |
| H(16)–N(1)–H(17) | 94(6) |
| S(1)–C(1)–C(15) | 111.8(4) |
| S(1)–C(2)–C(3) | 116.1(4) |
| S(2)–C(9)–C(7) | 115.7(4) |
| S(2)–C(10)–C(11) | 112.4(4) |

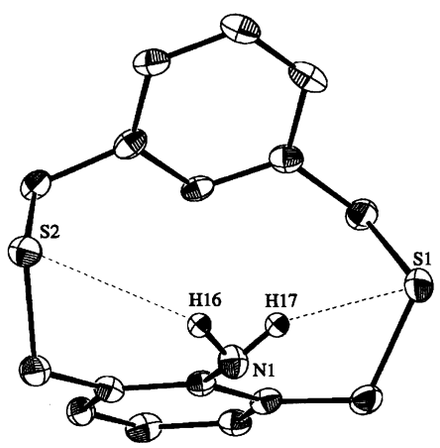


**Fig. 1** ORTEP drawing of aminodithia[3.3]MCP **6**. Hydrogen-bonding is shown by dotted lines.

monoamino[3.3]MCP **6** appeared in the upfield region ($\delta$ = 4.93 ppm) compared with that of mononitroMCP **4** ($\delta$ = 7.36 ppm). This indicates that the internal aryl proton of MCP **6** is affected by the ring current effect of the opposite aromatic ring. This aromatic proton points toward the opposite aromatic ring. These results suggest that conformation of MCP **6** is not the *syn*-form.

In the IR spectra, the absorption wavenumbers of the symmetric and asymmetric stretching vibrations of the amino group in monoaminoMCP **6** appeared at 3390 and 3322 cm$^{-1}$, respectively. On the other hand, the corresponding absorptions of aminonitroMCP **8** were observed at 3450 and 3361 cm$^{-1}$, respectively. MCP **6** thus shows values that are 60 and 39 cm$^{-1}$ lower than those of MCP **8**. In MCP **7**, three absorptions for the amino groups appeared at 3395, 3375 and 3320 cm$^{-1}$. These results strongly indicate the existence of hydrogen-bonding in these structures.

In order to confirm in more detail the formation of hydrogen-bonds, X-ray structural analyses of aminoMCPs **6** and **7** were performed at low temperature. The selected bond lengths and bond angles for MCP **6** and MCP **7** are summarized in Tables 2 and 3, respectively. The molecular structures are shown in Figs. 1 and 2. Intramolecular hydrogen-bonding between amino protons and bridge sulfur atoms is indicated by dotted lines. The conformation of monoaminoMCP **6** is not *syn* but *anti*. The distances and angles involved in the hydrogen-bonding between the amino protons and the bridge sulfur atoms in monoaminoMCP **6** are 2.81 (137(7)°) (N1–H16 ··· S2) and 2.79 Å (128(5)°) (N1–H17 ··· S1), respectively. The distances between the amino nitrogen atom and bridge sulfur atoms in monoaminoMCP **6** are 3.44 (N1 ··· S2) and 3.45 Å (N1 ··· S1), respectively. In contrast, the distances and angles involved in the hydrogen-bonding between the amino protons and the bridge sulfur atoms in diaminoMCP **7** are 2.49 (144°) (N2–H15 ··· S2), 2.64 (132°) (N2–H16 ··· S1), 2.48 (143°) (N1–H17 ··· S1) and 2.70 Å (140°) (N1–H18 ··· S2), respectively. The distances between the amino nitrogen atoms and the bridge sulfur atoms in diaminoMCP **7** are 3.24 (N2 ··· S2), 3.35 (N2 ··· S1), 3.26 (N1 ··· S1) and 3.35 Å (N1 ··· S2), respectively. Interestingly, the two amino

**Table 3** Selected bond lengths (Å) and bond angles (°) for MCP **7**

| | |
|---|---|
| S(1)–C(1) | 1.836(2) |
| S(1)–C(2) | 1.835(2) |
| S(2)–C(9) | 1.835(2) |
| S(2)–C(10) | 1.844(2) |
| N(1)–C(8) | 1.401(3) |
| N(2)–C(16) | 1.397(3) |
| | |
| C(8)–N(1)–H(8) | 112(1) |
| C(8)–N(1)–H(9) | 115(1) |
| H(8)–N(1)–H(9) | 112(2) |
| C(16)–N(2)–H(17) | 112(1) |
| C(16)–N(2)–H(18) | 115(1) |
| H(17)–N(2)–H(18) | 111(2) |
| C(1)–S(1)–C(2) | 106.3(1) |
| C(9)–S(2)–C(10) | 106.3(1) |
| S(1)–C(1)–C(15) | 117.4(2) |
| S(1)–C(2)–C(3) | 116.4(1) |
| S(2)–C(9)–C(7) | 119.1(1) |
| S(2)–C(10)–C(11) | 116.0(1) |

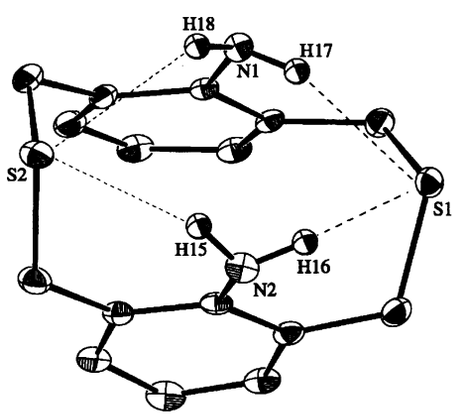


**Fig. 2** ORTEP drawing of diaminodithia[3.3]MCP **7**. Hydrogen-bonding is shown by dotted lines.

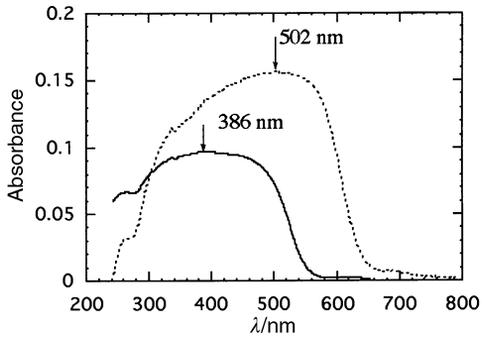


**Fig. 3** Solid state absorption spectra of polymorph **8-I** (line) and polymorph **8-II** (dotted line).

groups and the two sulfur atoms of MCP **7** are involved in the formation of a cyclic hydrogen-bonding network. In MCP **6**, the hydrogen-bonding network is less extended because it is restricted to occurring between one amino group and two sulfur atoms. Furthermore, the bridges of the thiaether groups ($-CH_2SCH_2-$) in both MCP **6** and MCP **7** are fixed as boat–boat structures in order to form the hydrogen-bonding network.

Aminonitrodithia[3.3]MCP **8** was recrystallized from dichloromethane–hexane to give two different polymorphs, that is, a red (**8-I**) and a yellow polymorph (**8-II**). Both prisms were identical in terms of their $^1$H-NMR and MS spectra. The red polymorph **8-I** changed to a yellow one at 168 °C on heating and melted at 223–225 °C. The two endothermic peaks were also confirmed by differential scanning calorimetry (DSC) measurements. Cooling of the yellow polymorph below 168 °C did not change it to the red one. This phenomenon was also observed when the polymorph **8-I** was exposed to the moisture (*ca.* 60–80%) at room temperature for about 3 weeks. Under a dry argon atmosphere, such a color change was not observed. But the influence of moisture on this color change is still not clear, and the resulting yellow polymorphs melted between 223 and 225 °C. Such a melting point is identical with that of the yellow polymorph **8-II**, which is obtained by recrystallization of MCP **8**.

Electronic spectral measurements in solid and solution were carried out in order to make clear this color change. The maximum absorption wavelengths of the two polymorphs are identical ($\lambda_{max}$ = 321nm) in $CHCl_3$ solution. In contrast, in the solid state the maximum absorption wavelengths of the polymorphs **8-I** and **8-II** appeared at 502 and 386 nm, respectively (Fig. 3). The difference ($\Delta\lambda_{max}$ = 116 nm) might stem from a different packing of molecules.

In order to discover the reason for such a transformation X-ray structural analyses for the two polymorphs (**8-I** and **8-II**) were performed. Selected bond lengths and bond angles for the red polymorph **8-I** and the yellow polymorph **8-II** are summarized in Tables 4 and 5, respectively. Although the yellow polymorph (**8-II**) could be studied at low temperature, the red polymorph (**8-I**) was investigated at room temperature because the crystal broke upon cooling. The molecular structure of the red polymorph **8-I** is shown in Fig. 4. Weak intramolecular hydrogen-bonding between one of the amino protons and one oxygen atom of the neighboring nitro group or one of the bridge sulfur atoms is indicated by dotted lines. The distances and angles involved in the hydrogen-bonding are 2.35 (130°) (N1–H16 ··· O1), 2.99 (N1 ··· O1) and 2.54 (103°) (N1–H16 ··· S2), 3.22 Å (N1 ··· S2), respectively. The values for the yellow polymorph **8-II** are 2.71 (97°) (N1–H16 ··· O1), 2.99 (N1 ··· O1) and 2.45 (143°) (N1–H16 ··· S1), 3.25 Å (N1 ··· S1), respectively.

Interestingly, the molecules of the polymorph **8-I** assemble as a one-dimensional array column, which is shown in Fig. 5. In the column, there is an alternate arrangement of the aniline rings (A) and the nitrobenzene rings (B) of the molecules in an AABBAABB pattern (Fig. 6). The intramolecular face-to-face distance in the molecular structure between the aniline ring (A) and the nitrobenzene ring (B) is *ca.* 3.61 Å. In contrast, the intermolecular face-to-face distance is *ca.* 3.88 Å. The driving force for formation of this molecular assembly is considered to be the intermolecular weak π–π interaction because the distance seems too long for a charge-transfer interaction. However, the one-dimensional array column was not observed for polymorph **8-II**, as shown in Fig. 7. Transformation from the

**Table 4** Selected bond lengths (Å) and bond angles (°) for MCP **8-I**

| | |
|---|---|
| S(1)–C(1) | 1.821(4) |
| S(1)–C(2) | 1.826(3) |
| S(2)–C(9) | 1.809(4) |
| S(2)–C(10) | 1.832(4) |
| N(1)–C(8) | 1.475(4) |
| N(2)–C(16) | 1.397(5) |
| N(1)–O(1) | 1.222(4) |
| N(1)–O(2) | 1.231(3) |
| | |
| C(16)–N(2)–H(15) | 121(3) |
| C(16)–N(2)–H(16) | 111(3) |
| H(15)–N(2)–H(16) | 103(4) |
| C(8)–N(1)–O(1) | 119.8(3) |
| C(8)–N(1)–O(2) | 116.6(3) |
| O(1)–N(1)–O(2) | 123.6(3) |
| C(1)–S(1)–C(2) | 106.5(2) |
| C(9)–S(2)–C(10) | 104.7(2) |
| S(1)–C(1)–C(15) | 115.3(3) |
| S(1)–C(2)–C(3) | 113.8(2) |
| S(2)–C(9)–C(7) | 117.0(2) |
| S(2)–C(10)–C(11) | 116.8(2) |

**Table 5** Selected bond lengths (Å) and bond angles (°) for MCP **8-II**

| | |
|---|---|
| S(1)–C(1) | 1.843(3) |
| S(1)–C(2) | 1.826(2) |
| S(2)–C(9) | 1.832(3) |
| S(2)–C(10) | 1.834(3) |
| N(1)–C(8) | 1.476(3) |
| N(2)–C(16) | 1.395(3) |
| N(1)–O(1) | 1.244(2) |
| N(1)–O(2) | 1.228(2) |
| | |
| C(16)–N(2)–H(15) | 117(1) |
| C(16)–N(2)–H(16) | 108(1) |
| H(15)–N(2)–H(16) | 116(2) |
| C(8)–N(1)–O(1) | 117.3(2) |
| C(8)–N(1)–O(2) | 119.5(2) |
| O(1)–N(1)–O(2) | 123.2(2) |
| C(1)–S(1)–C(2) | 105.5(1) |
| C(9)–S(2)–C(10) | 104.8(1) |
| S(1)–C(1)–C(15) | 116.0(2) |
| S(1)–C(2)–C(3) | 116.2(2) |
| S(2)–C(9)–C(7) | 113.7(2) |
| S(2)–C(10)–C(11) | 114.1(2) |

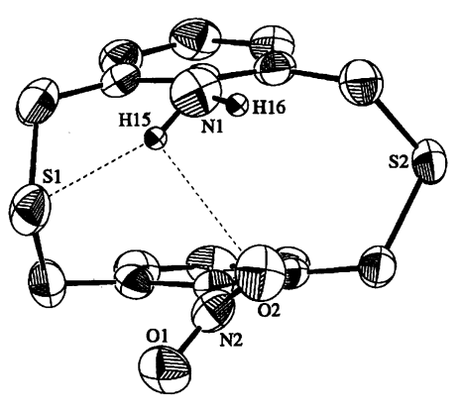


**Fig. 4** ORTEP drawing of aminodithia[3.3]MCP **8-I**. Hydrogen-bonding is shown by dotted lines.

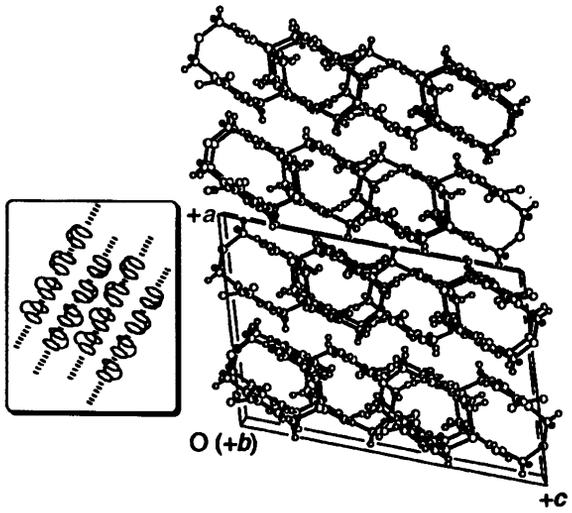


**Fig. 5** One-dimensional array columnar structure of the red polymorph **8-I**. Several of the columns were omitted for clarity.

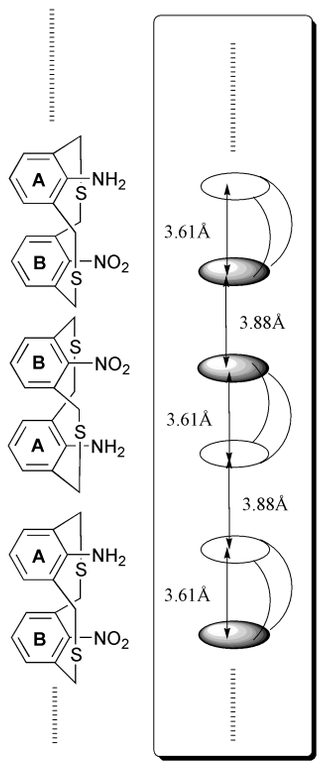


**Fig. 6** AABBAABB pattern in polymorph **8-I**.

polymorph **8-I** to the polymorph **8-II** can be presumed to occur as follows: half of the molecules in the one-dimensional array column rotate by *ca*. 90° and then the intermolecular hydrogen-bonds [2.39 Å (162°) (N1–H15 ··· O2*)] are formed between the rotated molecules and the non-rotated molecules in the neighboring column (Scheme 2).

The mounted sample of polymorph **8-I** on the gonio head of the X-ray apparatus turned yellow after 3 weeks at room temperature. X-Ray analysis was also carried out for the yellow sample and the resulting data were identical to those of polymorph **8-II**.

The calculated densities of **8-I** and **8-II** are 1.472 and 1.488 g $cm^{-3}$, respectively. These values are larger than those of the mono- and diaminodithia[3.3]MCPs (1.345 and 1.372 g $cm^{-3}$, respectively). Such high densities can be explained by intermolecular attractive forces such as intermolecular hydrogen-bonding or π–π interaction in both of the polymorphs of MCP **8**.

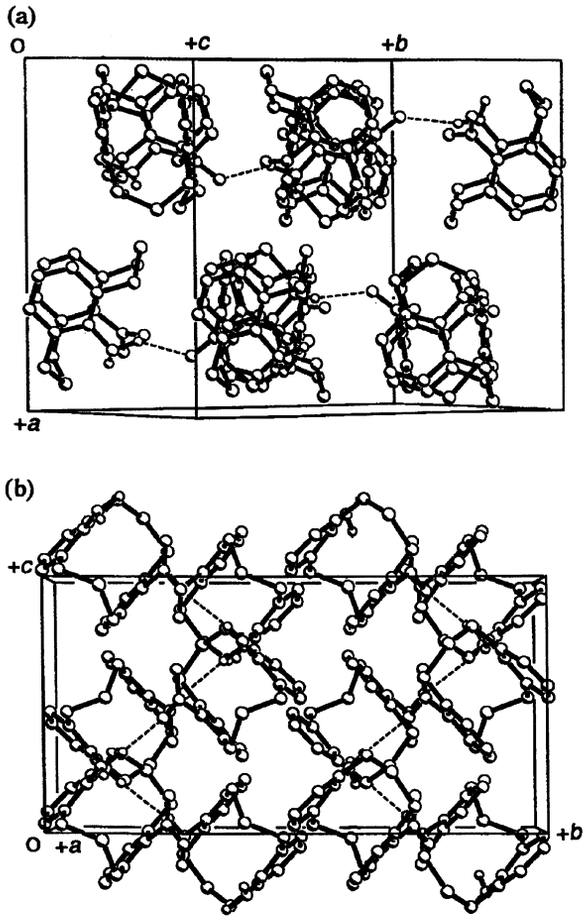


**Fig. 7** Crystal structure of polymorph **8-II** viewed (a) along the least-square axis and (b) along the *a* axis. Hydrogen atoms are omitted for clarity, with the exception of the amino protons, and hydrogen-bonding is shown by dotted lines.

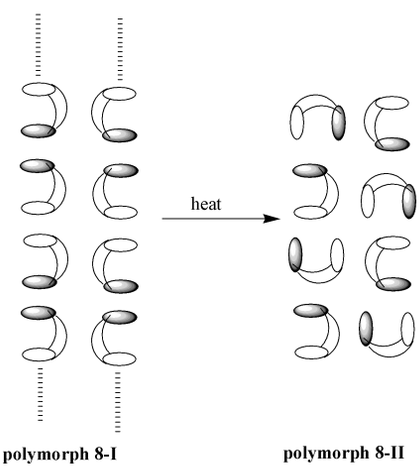


**Scheme 2**

## Conclusion

It can be concluded that the conformations of dithia[3.3]MCPs are affected not only by the steric hindrance of internal substituents, but also by the mode of intramolecular hydrogen-bonding. In particular, the formation of a cyclic hydrogen-bonding network is interesting in MCP **7**.

The crystal structure of MCP **8** is clearly affected by the intermolecular π–π interaction and the intermolecular hydrogen-bonding, resulting in occurrence of two polymorphs of the crystals. It is also noted that MCP **8** is readily, but irreversibly, converted from the red monoclinic polymorph **8-I**

to the yellow orthorhombic **8-II**. Furthermore, a long-range π–π interaction might exist along the one-dimensional array columnar axes in the the red polymorph **8-I**, judging from the fact that its maximum absorption wavelength is longer than that of the yellow polymorph **8-II** as found from measurements of their electronic spectra in the solid state.

## Experimental

All melting points were recorded on a Yanako hot-stage microscope apparatus and are uncorrected. $^1$H-NMR spectra were recorded on a Nippon Densi α-500 spectrometer and a Bruker AVANCE400S spectrometer in $CDCl_3$ with $Me_4Si$ as an internal reference. IR spectra were recorded on a Hitachi 260-30 spectrometer and a Nippon Bunko JASCO IR-700 spectrometer. Mass spectra were obtained on a Nippon Densi JEOL-DX-300 spectrometer at 75 eV using a direct inlet system. Differential scanning calorimetry (DSC) was carried out on a Shimadzu DSC-50 differential scanning calorimeter. Column chromatography was carried out on silica gel (Wako gel, C-300). The amount of silica gel used was 50–100 g. Absorption spectra were recorded on a Shimadzu UV-200S spectrometer for chloroform solutions at room temperature. Solid state absorption spectra were recorded on a Nippon Bunko JASCO V-550 spectrometer at room temperature.

### Preparation of *anti*-9-amino-2,11-dithia[3.3]metacyclophane 6

200 mg of 10% Pd/C were added to a solution of *syn*-9-nitro-2,11-dithia[3.3]metacyclophane **4** (200 mg, 0.63 mmol) in benzene (50 cm$^3$). After hydrogen gas had been introduced into the mixture, with stirring for 4 h at rt, the Pd/C was filtered off. The filtrate was evaporated under reduced pressure to leave the residue, which was recrystallized from benzene to give 164 mg (0.57 mmol, 91% yield) of **6** as colorless prisms, mp 170–171 °C; $\nu_{max}$(KBr)/cm$^{-1}$ 3390, 3322 ($NH_2$); $\delta_H$(500 MHz; $CDCl_3$) 3.39 (2H, d, $J$ = 14.3 Hz, $CH_2S$), 3.68 (2H, d, $J$ = 14.3 Hz, $CH_2S$), 3.82 (2H, d, $J$ = 13.7 Hz, $SCH_2$), 4.05 (2H, d, $J$ = 13.7 Hz, $SCH_2$), 4.93 (1H, s, aromatic), 6.75–6.90 (3H, m, aromatic), 7.03–7.08 (3H, m, aromatic); *m*/*z* 287 ($M^+$) (Found: C, 67.0; H, 5.9; N, 4.7%. Calcd for $C_{16}H_{17}NS_2$: C, 66.9; H, 6.0; N, 4.7%).

### Preparation of *syn*-9,18-diamino-2,11-dithia[3.3]metacyclophane 7

200 mg of 10% Pd/C were added to a solution of *syn*-9,18-dinitro-2,11-dithia[3.3]metacyclophane **5** (200 mg, 0.55 mmol) in benzene (50 cm$^3$). After hydrogen gas had been introduced into the mixture, with stirring for 6 h at rt, the Pd/C was filtered off. The filtrate was evaporated under reduced pressure to leave the residue, which was recrystallized from benzene to give 150 mg (0.50 mmol, 90% yield) of **7** as colorless prisms, mp 227–232 °C; $\nu_{max}$(KBr)/cm$^{-1}$ 3395, 3375, 3320 ($NH_2$); $\delta_H$(500 MHz; $CDCl_3$) 3.88 (4H, d, $J$ = 15.3 Hz, $CH_2S$), 4.14 (4H, d, $J$ = 15.3 Hz, $SCH_2$), 6.80–7.20 (6H, m, aromatic); *m*/*z* 302 ($M^+$) (Found: C, 63.7; H, 6.1; N, 9.2%. Calcd for $C_{16}H_{18}N_2S_2$: C, 63.5; H, 6.0; N, 9.3%).

### Preparation of *syn*-9-amino-18-nitro-2,11-dithia[3.3]metacyclophane 8

A stirred solution of **4** (50 mg, 0.14 mmol) and sodium hydrosulfide (100 mg, 1.8 mmol) in methanol (30 cm$^3$) and toluene (30 cm$^3$) was refluxed for 12 h under a stream of argon. The reaction mixture was poured into water and the organic layer was dried ($MgSO_4$) and evaporated under reduced pressure. The residue was chromatographed on a silica gel column with toluene as an eluent to give 21 mg (0.062 mmol, 45% yield) of **8** as a mixture of yellow and red prisms, mp 223–225 °C; $\nu_{max}$(KBr)/cm$^{-1}$ 3450, 3361 ($NH_2$); $\delta_H$(500 MHz; $CDCl_3$) 3.74 (2H, d, $J$ = 14.7 Hz, $CH_2S$), 3.83 (2H, d, $J$ = 15.3 Hz, $SCH_2$), 4.02 (2H, d, $J$ = 15.3 Hz, $SCH_2$), 4.46 (2H, d, $J$ = 14.7 Hz, $CH_2S$), 6.80–7.20 (6H, m, aromatic); *m*/*z* 332 ($M^+$) (Found: C, 57.8; H, 5.1; N, 8.5%. Calcd for $C_{16}H_{16}N_2O_2S_2$: C, 57.8; H, 4.9; N, 8.4%); $\lambda_{max}$/nm 321 ($\varepsilon$/dm$^3$ mol$^{-1}$ cm$^{-1}$ 230000).

### Crystal structure determinations of MCPs 6, 7, 8-I and 8-II †

**Crystal data for MCP 6.** Recrystallized from benzene. $C_{16}H_{17}NS_2$, $M_r$ = 287.44, monoclinic, $a$ = 7.892(2), $b$ = 15.17(2), $c$ = 12.017(4) Å, $\beta$ = 99.496(8)°, $V$ = 1419.24 Å$^3$, $P2_1/a$ (no. 14), $Z$ = 4, $\rho_{calc}$ = 1.345 g cm$^{-3}$, $T$ = 123 K, $R$ = 0.067, $R_w$ = 0.091; 2824 unique reflections with $2\theta \leq 55.6°$. Of these, 2519 $I > 3.00\ \sigma(I)$.

**Crystal data for MCP 7.** Recrystallized from benzene. $C_{16}H_{18}N_2S_2$, $M_r$ = 302.45, tetragonal, $a$ = 25.166(8), $b$ = 25.166(8), $c$ = 9.246(7) Å, $V$ = 5859.09 Å$^3$, $I4_1/a$ (no. 88), $Z$ = 16, $\rho_{calc}$ = 1.372 g cm$^{-3}$, $T$ = 93 K, $R$ = 0.040, $R_w$ = 0.043; 3309 unique reflections with $2\theta \leq 55.6°$. Of these, 3021 $I > 3.00\ \sigma(I)$.

**Crystal data for polymorph 8-I.** Recrystallized from benzene. $C_{16}H_{16}N_2O_2S_2$, $M_r$ = 332.43, monoclinic, $a$ = 13.021(2), $b$ = 12.276(2), $c$ = 19.352(1) Å, $\beta$ = 107.004(8)°, $V$ = 2998.9(6) Å$^3$, $C2/c$ (no. 15), $Z$ = 4, $\rho_{calc}$ = 1.472 g cm$^{-3}$, $T$ = 298 K, $R$ = 0.040, $R_w$ = 0.049; 2337 unique reflections with $2\theta \leq 120.1°$. Of these, 2047 $I > 3.00\ \sigma(I)$.

**Crystal data for polymorph 8-II.** Recrystallized from benzene. $C_{16}H_{16}N_2O_2S_2$, $M_r$ = 332.43, orthorhombic, $a$ = 14.345(6), $b$ = 20.103(6), $c$ = 10.291(8) Å, $V$ = 2967.76 Å$^3$, $Pbca$ (no. 61), $Z$ = 8, $\rho_{calc}$ = 1.488 g cm$^{-3}$, $T$ = 103 K, $R$ = 0.043, $R_w$ = 0.045; 3516 unique reflections with $2\theta \leq 55.6°$. Of these, 3114 $I > 3.00\ \sigma(I)$.

Intensity data for MCP **6**, **7** and polymorph **8-II** were collected on a Rigaku RAXIS-4 Imaging Plate with graphite-monochromated Mo-Kα radiation. Intensity data for polymorph **8-I** were collected on a Rigaku AFC-7R diffractometer with graphite-monochromated Cu-Kα radiation. These structures were solved with the teXsan crystallographic software package of the Molecular Structure Corporation. All hydrogen atoms were found from differential Fourier maps. XYZ and isotropic B factors of all amino protons were refined.

† CCDC reference numbers 112282, 112283, 115886, 116596. See http://www.rsc.org/suppdata/p2/b1/b100285f/ for crystallographic files in.cif or other electronic format.

## References


1 *Cyclophanes*, eds. P. M. Keehn and S. M. Rosenfeld, Academic Press, New York, 1983, vols. I and II; V. Boekelheide, *Topics in Current Chemistry*, ed. F. L. Boschke, Springer-Verlag, Berlin, 1987; F. Diederich, *Cyclophanes*, Royal Society of Chemistry, Cambridge, 1989; *Monographs in Supramolecular Chemistry*, ed. J. F. Stoddart, vol. 1, Royal Society of Chemistry, Cambridge, 1989, vol. 1; J.-M. Lehn, *Supramolecular Chemistry*, VCH, Weinheim, 1995; *Supramolecular Control of Structure and Reactivity*, ed. A. D. Hamilton, Wiley, Chichester, 1996.

2 T. Otsubo, M. Kitagawa and S. Misumi, *Bull. Chem. Soc. Jpn.*, 1979, **52**, 1515; M. F. Semmelhack, Y. Thebtaranonth and L. Keller, *J. Am. Chem. Soc.*, 1977, **99**, 959; T. Moriguchi, K. Sakata and A. Tsuge, *J. Chem. Res. (S)*, 1999, 605; T. Moriguchi, K. Sakata and A. Tsuge, *J. Chem. Res. (M)*, 1999, 2601; A. Tsuge, N. Takagi, T. Kakara, T. Moriguchi and K. Sakata, *Chem. Lett.*, 2000, 949.

3 K. Böckmann and F. Vögtle, *J. Chem. Res. (S)*, 1980, 192; K. Böckmann and F. Vögtle, *J. Chem. Res. (M)*, 1980, 2776.

4 K. Böckmann and F. Vögtle, *Chem. Ber.*, 1981, **114**, 1065.

5 R. H. Mitchell and V. Boekelheide, *J. Am. Chem. Soc.*, 1973, **96**, 1547.